Tran-SET

Transportation Consortium of South-Central States

Solving Emerging Transportation Resiliency, Sustainability, and Economic Challenges through the Use of Innovative Materials and Construction Methods: From Research to Implementation

Detection and Estimation of Inundation and Associated Risks Using Traffic Monitoring Cameras and Image Processing Under Extreme Flooding Conditions

Project No. 19SAUTA04

Lead University: The University of Texas at Arlington

Final Report

August 2020

Disclaimer

The contents of this report reflect the views of the authors, who are responsible for the facts and the accuracy of the information presented herein. This document is disseminated in the interest of information exchange. The report is funded, partially or entirely, by a grant from the U.S. Department of Transportation's University Transportation Centers Program. However, the U.S. Government assumes no liability for the contents or use thereof.

Acknowledgements

The authors acknowledge the Tran-SET for providing the financial support of this study. The authors also would like to thank Project Review Committee, Do Soo Moon, Jun Hak Lee, and Haksu Lee for their support and direction of the project.

TECHNICAL DOCUMENTATION PAGE

1. Project No.	2. Government Accession No.	3. Recipient's Catalog No.
19SAUTA04		

4. Title and Subtitle	5. Report Date
Detection and estimation of inundation and associated risks using traffic monitoring cameras and image processing under extreme flooding conditions	Aug. 2020
	6. Performing Organization Code

7. Author(s)	8. Performing Organization Report No.
PI: Dr. Suyun Ham (ORCID: 0000-0001-6375-211X) Co-PI: Dr. Seongjin Noh (ORCID: 0000-0002-2683-7269) Co-PI: Dr. Dong-Jun Seo (ORCID: 0000-0003-3863-8408) GRA: Yin Chao Yu GRA: Sangoo Kang	

9. Performing Organization Name and Address	10. Work Unit No. (TRAIS)
Transportation Consortium of South-Central States (Tran-SET) University Transportation Center for Region 6 3319 Patrick F. Taylor Hall, Louisiana State University, Baton Rouge, LA 70803	**11. Contract or Grant No.**

12. Sponsoring Agency Name and Address	13. Type of Report and Period Covered
United States of America Department of Transportation Research and Innovative Technology Administration	Final Research Report Aug. 2019 – Aug. 2020
	14. Sponsoring Agency Code

15. Supplementary Notes

Report uploaded and accessible at Tran-SET's website (http://transet.lsu.edu/).

16. Abstract

The main *objective* of this project is to develop an inundation detection and evaluation framework using images from traffic monitoring cameras and reliable flood monitoring under extreme precipitation conditions. This study presents a comparative assessment of image enhancement and segmentation techniques to automatically identify the flash flooding from the low-resolution images taken by traffic-monitoring cameras. Due to inaccurate equipment in severe weather conditions (e.g., raindrops or light refraction on camera lenses), low-resolution images are subject to noises that degrade the quality of information. De-noising procedures are carried out for the enhancement of images by removing different types of noises. After the de-noising, image segmentation is implemented to detect the inundation from the images automatically. In addition, the detection of the inundation using the image segmentation with and without de-noising techniques are compared. *The results* indicate that among de-noising methods, the Bayes shrink with the thresholding discrete wavelet transform shows the most reliable result. For the image segmentation, the Bayesian segmentation is superior to the others. The results demonstrate that the proposed image enhancement and segmentation methods can be effectively used to identify the inundation from low-resolution images taken in severe weather conditions. A new Bayesian filtering method will be devised and applied to estimate the inundation from low-resolution images that will allow traffic engineers to take preventive or proactive actions to improve the safety of drivers and protect and preserve the transportation infrastructure. This new observation with improved accuracy will enhance our understanding of dynamic urban flooding by filling an information gap in the locations where conventional observations have limitations.

17. Key Words	18. Distribution Statement
Inundation; Image processing; Bayes shrink; CCTV application	No restrictions. This document is available through the National Technical Information Service, Springfield, VA 22161.

19. Security Classif. (of this report)	20. Security Classif. (of this page)	21. No. of Pages	22. Price
Unclassified	Unclassified	33	

Form DOT F 1700.7 (8-72) **Reproduction of completed page authorized.**

SI* (MODERN METRIC) CONVERSION FACTORS

APPROXIMATE CONVERSIONS TO SI UNITS

Symbol	When You Know	Multiply By	To Find	Symbol
		LENGTH		
in	inches	25.4	millimeters	mm
ft	feet	0.305	meters	m
yd	yards	0.914	meters	m
mi	miles	1.61	kilometers	km
		AREA		
in^2	square inches	645.2	square millimeters	mm^2
ft^2	square feet	0.093	square meters	m^2
yd^2	square yard	0.836	square meters	m^2
ac	acres	0.405	hectares	ha
mi^2	square miles	2.59	square kilometers	km^2
		VOLUME		
fl oz	fluid ounces	29.57	milliliters	mL
gal	gallons	3.785	liters	L
ft^3	cubic feet	0.028	cubic meters	m^3
yd^3	cubic yards	0.765	cubic meters	m^3
		NOTE: volumes greater than 1000 L shall be shown in m^3		
		MASS		
oz	ounces	28.35	grams	g
lb	pounds	0.454	kilograms	kg
T	short tons (2000 lb)	0.907	megagrams (or "metric ton")	Mg (or "t")
		TEMPERATURE (exact degrees)		
^oF	Fahrenheit	5 (F-32)/9 or (F-32)/1.8	Celsius	^oC
		ILLUMINATION		
fc	foot-candles	10.76	lux	lx
fl	foot-Lamberts	3.426	$candela/m^2$	cd/m^2
		FORCE and PRESSURE or STRESS		
lbf	poundforce	4.45	newtons	N
lbf/in^2	poundforce per square inch	6.89	kilopascals	kPa

APPROXIMATE CONVERSIONS FROM SI UNITS

Symbol	When You Know	Multiply By	To Find	Symbol
		LENGTH		
mm	millimeters	0.039	inches	in
m	meters	3.28	feet	ft
m	meters	1.09	yards	yd
km	kilometers	0.621	miles	mi
		AREA		
mm^2	square millimeters	0.0016	square inches	in^2
m^2	square meters	10.764	square feet	ft^2
m^2	square meters	1.195	square yards	yd^2
ha	hectares	2.47	acres	ac
km^2	square kilometers	0.386	square miles	mi^2
		VOLUME		
mL	milliliters	0.034	fluid ounces	fl oz
L	liters	0.264	gallons	gal
m^3	cubic meters	35.314	cubic feet	ft^3
m^3	cubic meters	1.307	cubic yards	yd^3
		MASS		
g	grams	0.035	ounces	oz
kg	kilograms	2.202	pounds	lb
Mg (or "t")	megagrams (or "metric ton")	1.103	short tons (2000 lb)	T
		TEMPERATURE (exact degrees)		
^oC	Celsius	1.8C+32	Fahrenheit	^oF
		ILLUMINATION		
lx	lux	0.0929	foot-candles	fc
cd/m^2	$candela/m^2$	0.2919	foot-Lamberts	fl
		FORCE and PRESSURE or STRESS		
N	newtons	0.225	poundforce	lbf
kPa	kilopascals	0.145	poundforce per square inch	lbf/in^2

TABLE OF CONTENTS

TECHNICAL DOCUMENTATION PAGE ii
TABLE OF CONTENTS iv
LIST OF FIGURES v
LIST OF TABLES vi
ACRONYMS, ABBREVIATIONS, AND SYMBOLS vii
EXECUTIVE SUMMARY viii
1. INTRODUCTION 1
2. OBJECTIVES AND APPROACH 2
3. PROCEDURE 4
4. FINDINGS 14
REFERENCES 25
APPENDIX: Analysis data and filtered data 28

LIST OF FIGURES

Figure 1. The basic flowchart of this study for inundation detection. (1) Collect closed-circuit television (CCTV) images from government websites or social media; (2) use four different de-noising filterings to find out which has the best de-noising quality, which evaluated by the peak signal-to-noise ratio (PSNR); (3) use image segmentation methods to understand how the computer interprets images and finds an edge which is the vital part for image object detection; (4) compare segmentation results between each method and detect inundation area..... 5

Figure 2. The example images with three different types of noises. (a) The Gaussian noise; (b) the impulse noise; and (c) the speckle noise.....**Error! Bookmark not defined.**

Figure 3. The scale decomposition of discrete wavelet transforms: (a) the first scale decomposition of a discrete wavelet transform representing each wavelet coefficient in a spatial area corresponding to approximately a 2 × 2 area of the original image and (b) an n-scale wavelet decomposition.....**Error! Bookmark not defined.**

Figure 4. The basic framework of wavelet image de-noising. It shows the process of wavelet de-noising. There are three main steps. 1) Apply wavelet transform to image data and calculate the wavelet coefficients. 2) Find the optimum value for threshold and applying a soft threshold. 3) Calculate the de-noised signal and reconstruct the image. .....**Error! Bookmark not defined.**

Figure 5. Example images used for inundation detection experiments which are No. 1 to No. 6 in Table 1 collected from CCTV and social media used in this paper. (a) and (b) are flooded roads during Hurricane Harvey collected from CCTV; others are collected from social media.**Error! Bookmark not defined.**

Figure 6. The results of CCTV image (Case No.1 in Figure 6) via different de-noising methods: (a) Original CCTV image; (b) an image by using Bayes shrink; (c) an image by using Arithmetic filtering; (d) an image by using Median filtering and (e) an image by using Gaussian filtering. (b) Bayes shrink is the best of these de-noising method for CCTV images. It not only removes the noise but also retains important information, including brightness, color, and resolution of the original image. 15

Figure 7. The chart of PSNR for each method with different 14 CCTV images..... 18

Figure 8. The comparison of before and after image de-noising filtering using different image segmentation methods..... 19

Figure 9. Inundation detection based on the results of Bayesian segmentation. 20

Figure 10. The matching image with edge detection based on Bayesian segmentation result and original CCTV image.....**Error! Bookmark not defined.**

LIST OF TABLES

Table 1. The PSNR of each de-noising filtering 17

ACRONYMS, ABBREVIATIONS, AND SYMBOLS

CCTV	closed-circuit television
DWT	discrete wavelet transform
FFT	fast Fourier transform
MSE	mean squared error
PSNR	peak signal-to-noise ratio
ROI	region of interest

EXECUTIVE SUMMARY

The extreme weather such as Hurricane Harvey is one of the most severe natural disasters which threatens the safety and resiliency of the communities and transportation infrastructure in Region 6. In the face of natural disasters such as flash flooding, prompt information is crucial to establish a mitigation plan and find the best route for first responders. These rains cause unprecedented flooding and cause severe fatalities and hundreds of billions of US dollars in damages. Such an extreme flood not only damages roads and bridges but also cuts off evacuation routes and rescue paths. In many parts of the US, occurrences of "rare" extreme precipitation and flooding events are now a new normal *(1)*.

A new Bayesian filtering method will be devised and applied based on a comparative assessment of image enhancement and segmentation techniques to automatically identify the flash flooding from the low-resolution images taken by traffic-monitoring cameras. Due to inaccurate equipment in severe weather conditions (e.g., raindrops or light refraction on camera lenses), low-resolution images are subject to noises that degrade the quality of information. De-noising procedures are carried out for the enhancement of images by removing different types of noises. For the comparative assessment of de-noising techniques, the Bayes shrink and three conventional methods are compared. After the de-noising, image segmentation is implemented to detect the inundation from the images automatically. For the comparative assessment of image segmentation techniques, k-means segmentation, Otsu segmentation, and Bayesian segmentation are compared. In addition, the detection of the inundation using the image segmentation with and without de-noising techniques are compared.

The results indicate that among de-noising methods, the Bayes shrink with the thresholding discrete wavelet transform shows the most reliable result. For the image segmentation, the Bayesian segmentation is superior to the others. The results demonstrate that the proposed image enhancement and segmentation methods can be effectively used to identify the inundation from low-resolution images taken in severe weather conditions. By using the principle of the image processing presented in this paper, we can estimate the inundation from images and assess flooding risks in the vicinity of local flooding locations. Such information will allow traffic engineers to take preventive or proactive actions to improve the safety of drivers and protect and preserve the transportation infrastructure. This new observation with improved accuracy will enhance our understanding of dynamic urban flooding by filling an information gap in the locations where conventional observations have limitations.

1. INTRODUCTION

The extreme weather such as Hurricane Harvey is one of the most severe natural disasters which threatens the safety and resiliency of the communities and transportation infrastructure in Region 6. The 3-day rainfall in parts of Houston and the storm total rainfall by Harvey are estimated to have return periods of over 9,000 and 2,000 years, respectively, which exceed the amount of a design storm for roadways. These rains caused unprecedented flooding and caused over 70 fatalities and $ 125 billion US dollars in damages, making Harvey the second-costliest hurricane in US history. Such an extreme flood not only damages roads and bridges but also cuts off evacuation routes and rescue paths. In many parts of the US including Region 6, occurrences of "rare" extreme precipitation and flooding events are now a new normal. Although transportation infrastructure is designed and managed according to low-frequency flood standards (e.g., 50-yr or 100-yr return flood), an increasing frequency of extreme precipitation and flooding events in recent years makes sustainable management of transportation infrastructure challenges. In addition, the conventional flood maps made under the stationary and fluvial flooding (i.e., inundation of river flow) assumptions are known as a poor predictor of the location of damaging flooding.

During the extreme flooding, photo images from traffic monitoring cameras provide critical information, sometimes as the only reliable source, to identify whether or not a road is flooded. The advent of new image processing and filtering technologies has enabled us to extract the extent of inundation from low-resolution photos with reasonable accuracy. Despite the high potential, however, the images from traffic monitoring systems have yet to be investigated to extract more accurate flood information using objective and automatic ways. Once the flooding is detected on the roads, it is crucial to estimate the spatial impact of local flooding to highways and roads in the vicinity to establish a traffic control plan and find the best route for the first responders.

The main goal of this project is to develop an inundation detection and evaluation framework using images from traffic monitoring cameras and image processing under extreme precipitation conditions. The framework aims at real-time applications to all sites where they are monitored by road traffic cameras. A major outcome of this project will be studied on filtering and image process methods to estimate the inundation from low-resolution images taken by the existing road traffic monitoring cameras to assess flooding risks in the vicinity of the local flooding locations, which meets transportation departments' goals and objectives of transportation safety in an urban area and Region 6.

2. OBJECTIVES AND APPROACH

2.1 Objective

The main objective of this project is 1) to develop an inundation detection and 2) evaluate a framework using images from traffic monitoring cameras under extreme precipitation conditions. Comparative assessment of developed image processing, including de-nosing and segmentation techniques, will be performed to estimate the inundation from low-resolution images taken by the existing road traffic monitoring cameras. The location and edge of inundation in the closed-circuit television (CCTV) image can be estimated by Bayesian filtering.

To fulfill the objectives of the project, the tasks of this project are:

1. Comprehensive literature review regarding existing methodologies of image processing which are de-nosing filtering and image segmentation.
2. Development of a new Bayesian filtering based on the concept of image processing to detect inundation area from images.
3. Estimation of Inundation from actual traffic monitoring images: Does the developed Bayesian filtering successfully identify the occurrence of inundation from road traffic monitoring images?
4. Comparative assessment of developed Bayesian filtering method with other de-nosing and segmentation techniques to verify the inundation detection reliability of the proposed method.

2.2. Approach and Literature Review

In the face of natural disasters such as flash flooding, prompt information is crucial to establish a mitigation plan and find the best route for first responders. These rains cause unprecedented flooding and cause severe fatalities and hundreds of billions of US dollars in damages. Such an extreme flood not only damages roads and bridges but also cuts off evacuation routes and rescue paths *(1)*. There are different types of observations to monitor and detect floods in urban areas. Among them, typical measurement methods include in-situ water level sensors in streams, remote sensing from satellites and airborne drones, on-site images from social media, and traffic-monitoring systems. Each observation type contributes to filling the information gap to grasp a holistic picture of urban flooding with different spatiotemporal scales. Despite the advance in measurement techniques, there are still limitations known for each measurement approach. For instance, in-situ water-level sensors are adapted to only stream monitoring. Instrumenting entire hydrological basins, which can cover hundreds of square kilometers, is practically and economically infeasible. Satellites are still limited to monitoring water levels and flow remotely with a low temporal frequency. Optical measurements from satellites and drones allow measuring only in a short period, and they are impossible during floods with severe weather conditions. For example, thick cloud layers interfere with the observation of satellites, while drones cannot fly when the wind is strong.

The vertical resolution of current synthetic aperture radars (tens of centimeters) with several days of the repeat cycle is insufficient for the task *(2,3)*. Without promising real-time flooding information, local citizens face the possible danger of tragedies. To address those limitations, effective, inexpensive, and reliable approaches are needed instead of installing additional facilities

or equipment to detect flooding or inundation near civil infrastructure (e.g., highways and bridges). On-site images from traffic monitoring systems which are automatically photographed at regular times provide critical information for citizen and government, sometimes as the only reliable and practical sources, to identify the occurrence of flooding under extreme weather conditions in real-time, and protect people from exposure to danger for taking pictures in these conditions *(4)*. Despite these advantages, low-resolution images such as closed-circuit television (CCTV) photos are often corrupted by noises that can degrade image quality due to transmission or capture by inaccurate equipment or natural weather environments (e.g., raindrops or light refraction on camera lenses). The low-resolution images from traffic monitoring cameras or CCTV are one of the few reliable sources to know the outside conditions during extreme natural disasters *(5,6)*.

The low resolution creates a dilemma to be overcome; for example, there are monitors in different places such as intersections or highways, but the resolution of CCTV is not fine enough for decision-makers to use the footage to decide to evacuate people to a safe place or guide a correct route for transportation. In addition, it is challenging to detect inundation from CCTV images using only a deep learning approach, which is one of the common applications of object detection. However, it requires many images sources in the same position but different situations to form the training database *(7)*. Unless the rain is heavy enough to quickly accumulate water on the road that can be recorded by erected equipment at the same time, it is difficult to obtain water levels changing with obvious differences in the image. From the context of the recognition target, detecting inundation from an image is different from the conventional image processing or target tracking procedure. In the conventional image processing, the water in an image may be regarded as noise or unnecessary background to be removed to better recognize common objects of interest such as cars or humans. For the detection of inundation, on the contrary, the edge of water bodies with changing boundaries and reflectivity is the object of interest to be recognized in while the other objects, but the water needs to be filtered out.

The de-noising filtering method is used to enhance the quality of an image by removing noises mixed in when the image is digitized and reconstructing a signal in the original image by extracting features in the image *(8)*. The impact of image noise can be decreased by changing the pixels to adjust brightness and contrast with the de-noising filtering methods (e.g., mean filtering and median filtering) *(9)*. In recent years, engineering communities have developed de-noising technologies *(8,10)*. Thresholding discrete wavelet transform (DWT) coefficients have been mainly studied for de-noising *(11–13)*. The wavelet is usually calculated by using spatial Gaussian variables, while different wavelets are derived from different Gaussian multi-order derivative functions *(14,15)*. The principal of the wavelet coefficient is to set a processing range by a threshold to achieve de-noising *(16)*. The wavelet coefficients method has the characteristics of bandpass filtering. Thus, the use of the wavelet decomposition and reconstruction method allows feasible de-noising *(17,18)*. Since wavelet coefficients for de-noising are well-studied, many threshold approaches have been proposed. Among those threshold methods, the wavelet Bayes shrink approach is the most effective wavelet coefficient method *(14)*. Based on Bayesian theory, the Bayes shrink is changed according to different image information, so the Bayes shrink is also called the adaptive threshold *(15,19)*. The most important concept of de-noising is that there is no best de-noising method, but only the most suitable de-noising method because the noise of each image is different. Thus, it is important to test and choose the most accurate de-noising filtering for a CCTV image to enhance image segmentation, which allows estimating the inundated area.

Image segmentation is one of the hotspots in image processing and computer vision, which is the basis for image analysis and understanding of image feature extraction and recognition. It refers to dividing the image into several areas based on grayscale, color, texture, and shape. The features divided into the same area are similar, and there are significant differences between different areas. There is a common principle in image segmentation algorithms which can be divided to region-based segmentation, edge detection segmentation, and clustering segmentation. Dijk and Hollander *(20)* describe each algorithm in unified frameworks that introduce separate clusters and data weight functions. Felzenszwalb and Huttenlocher *(21)* study two different local neighborhoods in constructing the graph, by which the important characteristic of the method is its ability to preserve detail.

In this study, a new Bayesian filtering method used for image segmentation is developed and compared with different image segmentation methods, including k-means clustering segmentation, Otsu region-based segmentation to presents an effective image-processing procedure that requires only a single image to detect the inundation area in a CCTV image to overcome limitations on current flooding detection.

3. PROCEDURE

On-site images from traffic monitoring systems which are automatically photographed at regular times provide critical information for citizen and government, sometimes as the only reliable and practical sources, to identify the occurrence of flooding under extreme weather conditions in real-time, and protect people from exposure to danger for taking pictures in these conditions *(4)*.

Despite these advantages, low-resolution images such as closed-circuit television (CCTV) photos are often corrupted by noises that can degrade image quality due to transmission or capture by inaccurate equipment or natural weather environments (e.g., raindrops or light refraction on camera lenses). The low-resolution images from traffic monitoring cameras or CCTV are one of the few reliable sources to know the outside conditions during extreme natural disasters *(5,6)*.

To address the challenges to detect inundation in CCTV images using other approaches including a neural network, the project *proposed 1) de-noising and 2) image segmentation approach to find the water area in the image by de-noising and image segmentation.* The first step is to find the most suitable de-noising method for CCTV images in Section 3.1. The second step is to use image segmentation to find the edge further to find the water or inundation area in the image in Section 3.2. The flowchart of this study is shown in Figure 1. The effectiveness of de-noising is determined by the peak signal-to-noise ratio (PSNR), which is commonly used for image compression and reconstruction after image de-noising. The higher the PSNR, the better the de-noising effect, and the more original image information is retained.

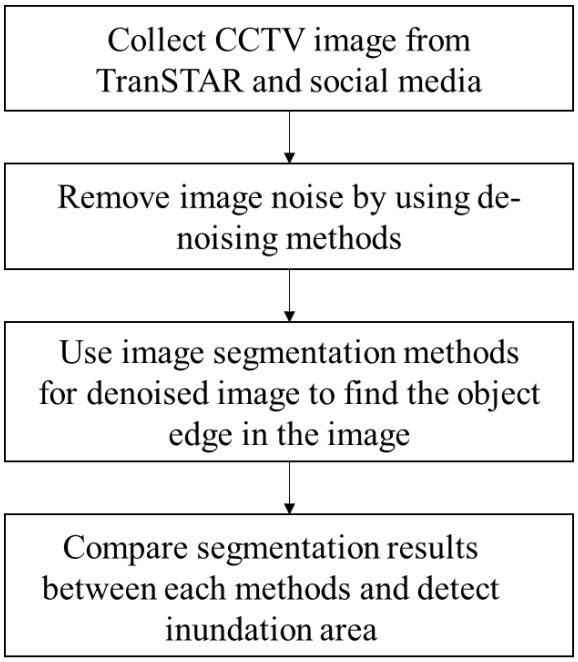

Figure 1. The basic flowchart of this study for inundation detection. (1) Collect closed-circuit television (CCTV) images from government websites or social media; (2) use four different de-noising filterings to find out which has the best de-noising quality, which evaluated by the peak signal-to-noise ratio (PSNR); (3) use image segmentation methods to understand how the computer interprets images and finds an edge which is the vital part for image object detection; (4) compare segmentation results between each method and detect inundation area.

In image processing, practically we face various random noises. They are distributed in the CCTV image, caused by digitized transmission compression or equipment, which affects the performance of image processing. There are two requirements for the de-noising filtering: keeping intact important information (e.g., the object edges) and making the image clearer with a better visual impact so the image's information can be clearly seen. We will study several de-noising filtering techniques: mean filtering, and median filtering, which belong to image enhancement. The performance of the de-noising method depends on the type of noise. For example, median de-noising filtering is very effective in smoothing impulse noise while it allows keeping the sharp edges of the image. The results of the image segmentation to find inundation objects edge effectively and accurately by de-noising filtering.

To find out which type of de-noising method is the most suitable for flood identification from CCTV images, we need to understand the type of noise. During image acquisition, encoding, transmission, and processing steps, noise always appears in the digital image. Without prior knowledge of filtering techniques, it is difficult to remove noise from digital images. Image noise is a random change in brightness or color information in the captured image. It is degradation in image signal caused by external sources. We can model a noisy image as $A(x, y) = H(x, y) + B(x, y)$ where, $A(x, y)$ is a function of the noisy image, $H(x, y)$ is a function of image noise, and $B(x, y)$ is a function of the original image. Before de-noising, we need to understand which noises are in the image. There are different types of image noise. They are typically divided into 3 types, which are Gaussian noise, impulse noise, and speckle noise. Gaussian noise is generated by adding a random Gaussian function to the image, while impulse noise is caused by adding random white and black dots to the image, and speckle noise is a granular noise that inherently exists in an image

and reduces its quality. An example of adding noise to the image is shown in Figure 2. Due to the wide variety of image noise, it is necessary to test different de-noising methods separately to determine the most suitable de-noising method for CCTV images.

(a) Gaussian noise (b) Impulse noise

(a) Speckle noise

Figure 2. The example images with three different types of noises. (a) The Gaussian noise; (b) the impulse noise; and (c) the speckle noise.

3.1 De-Noising Method

The image enhancement is performed by changing the pixel number of images with several convolution approaches (e.g., spatial convolution and frequency convolution), which is a mathematical operation to determine a new pixel value from a linear combination of pixel values and its neighboring pixels. The spatial convolution is simply calculated by arithmetic, such as add, minus, multiply, and divide pixel value. The frequency convolution is calculated by the information of the image after the fast Fourier transform (FFT), which converts the information from the spatial domain to a frequency domain *(22)*. The principle of image enhancement is to modify pixels by changing the brightness, contrast, and simply de-noising *(23)*.

3.1.1 Median Filtering and Arithmetic Filtering

If a signal changes gently, the output value, which are pixels of images, can be replaced by the statistical median value in a certain size neighborhood of this pixel point, and this neighborhood is called a window in the signal-processing field. The larger the window, the smoother the output, but it may also erase useful signal characteristics *(24)*. In order to keep the useful signal, the size of the window should be determined according to the signal and noise characteristics. Usually, the size of the window is odd because the odd number of data (e.g., pixel number) has a unique median value. The concept of mean filtering is similar to median filtering; the only difference is that the former uses the arithmetic mean as a filter *(25)*.

3.1.2 Gaussian Filtering

Gaussian filtering is commonly used as a linear filtering algorithm. A two-dimensional Gaussian function distribution is used to make a smooth image. The principle of Gaussian filtering is the weighted average of all pixel values in the entire image through the Gaussian distribution. More precisely, Gaussian filtering is the result of convolution operation on pixels by Gaussian normal distribution *(26)*. The value of each pixel is obtained by a weighted average of the values of itself and nearby pixels. The two-dimensional Gaussian function is:

$$\boldsymbol{G(x,y)} = \frac{\mathbf{1}}{\mathbf{2\pi\sigma^2}} \boldsymbol{e}^{\frac{-(x^2+y^2)}{2\sigma^2}} \quad (1)$$

where x and y are the number of pixels on the x and y-axis of the image, respectively and σ is the standard deviation of a Gaussian distribution.

3.1.3 Wavelet Coefficients

The discrete wavelet transform (DWT) can be interpreted as signal decomposition in a set of independent, spatially oriented frequency channels. "Signal decomposition" means that the signal passes through two complementary filters (e.g., low-pass and high-pass filters) and appears in the form of approximate and detailed signals as known as wavelet coefficients *(27)*. The approximate and detailed signals can be assembled back into the original signal without loss of information. The process is called reconstruction. The wavelet coefficients de-noising approach is based on signal decomposition. In this decomposition process, the image is divided into four sub-bands, as shown in Figure 3(a). The image is divided into four different sub-band based on their frequency. The four sub-band come from the separable application of vertical and horizontal directions. Each wavelet coefficient represents a spatial area corresponding to approximately a 2 × 2 area (see Figure 3) of the original image. The 2 × 2 spatial area as known as sub-band doesn't mean the image divided by horizontal and vertical line crossing on the center but means image decomposed by low-pass and high-pass filters. Each coefficient in the sub-bands represents a spatial area corresponding to approximately a 2×2 area of the original image. The frequencies ω can be divided into two ranges, the low-frequency range $(0 < |\omega| < \frac{\pi}{2})$ and high frequency range $(\frac{\pi}{2} < |\omega| < \pi)$. The sub-band labeled L or H depends on their frequency; L is low-frequency and H is

how-frequency. The four sub-band come from the separable application of vertical and horizontal direction. These four sub-band present image information called details: HH_1 is diagonal detail, LH_1 is vertical detail, HL_1 is horizontal detail and LL_1 is the remaining image details, where number 1 means detail in the first scale decomposition *(28)*. To obtain the next more critical scale of wavelet coefficients, the sub-band LL_1 is further decomposed, as shown in Figure 3(b). The image is divided into four different sub-band based on their frequency, which low frequency range in the second scale is $0 < |\omega| < \frac{\pi}{2^2}$ while high frequency range in second scale is $\frac{\pi}{2^2} < |\omega| < \frac{\pi}{2^1}$. Each coefficient in the sub-bands of the second scale HH_2, LH_2, HL_2, and LL_2 represent a spatial area corresponding to approximately a $2^2 \times 2^2$ area of the original picture. The decomposition process continues until a certain final scale is reached, while the degree of matching between the reconstructed signal and the original signal is 90%. The DWT shows the wavelet analysis is a measure of similarity between basis wavelets and the signal function *(29)*. The wavelet coefficients for image de-noising is the process of decomposition and reconstruction of details.

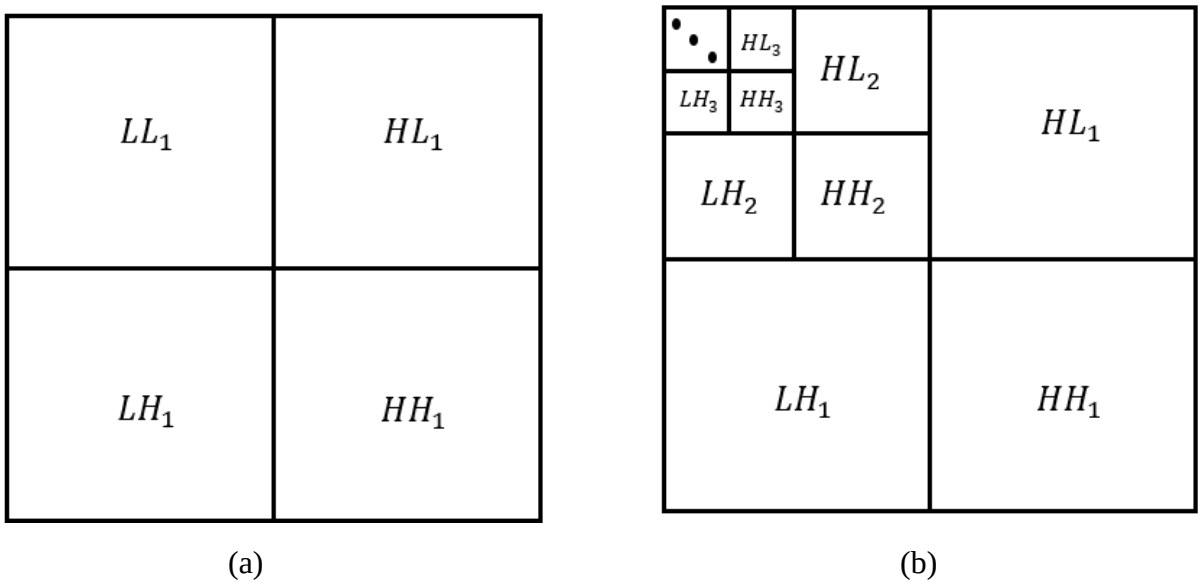

Figure 3. The scale decomposition of discrete wavelet transforms: (a) the first scale decomposition of a discrete wavelet transform representing each wavelet coefficient in a spatial area corresponding to approximately a 2 × 2 area of the original image and (b) an n-scale wavelet decomposition. The image is divided into four different sub-bands based on their frequency. Each coefficient in the sub-bands of the second scale HH_2, LH_2, HL_2, and LL_2 represent a spatial area corresponding to approximately a $2^2 \times 2^2$ area of the original image

The wavelet threshold is the reference point to divide the frequency of the image sub-band. The image and noise have different characteristics after wavelet transform. After the noisy signal is decomposed in the wavelet scale, the information of the image is mainly concentrated on the low-resolution sub-bands *(30)*, and the noise signal is mainly distributed on each high-frequency sub-bands. Thus, the choice of wavelet threshold directly affects the performance of wavelet de-noising. The wavelet coefficients of each scale are classified according to different threshold algorithms they used *(29)* If the wavelet coefficients are smaller than the threshold, set it to zero; otherwise, it maintains or slightly decreases the magnitude *(34)*. Because of this characteristic of wavelet coefficients, it is very effective in energy compression. The "energy compression" is as known as the process to save information or detail of image (e.g. color), which can better save

important image features such as edge changes in the image. Finding an optimal threshold is a tedious process. If using a smaller threshold, it produces a poor performance of de-noising, while using a larger threshold also causes image details to be removed as noise *(15)*.

In this project, Bayes shrink is used for wavelet coefficients, which has the best performance of de-noising for high-frequency noise *(19)*. The following is the Bayes shrink algorithm introduction. The Bayes shrink is known to be effective for images with Gaussian noise. The observation model is expressed as follows:

$$Y(i,j) = X(i,j) + V(i,j), \tag{2}$$

where Y is the wavelet transform of the noisy image; X is the wavelet transform of the original image, and V denotes the wavelet transform of the noise components following the Gaussian distribution $N(0, \sigma_v^2)$. Since X and V are mutually independent, the variances σ_y^2, σ_x^2 and σ_v^2 of Y, X and V is given by:

$$\sigma_y^2 = \sigma_x^2 + \sigma_v^2 \tag{3}$$

It has been shown that the noise variance σ_y^2 can be estimated from the first decomposition level diagonal high-frequency sub-band, HH_1 by the robust and accurate median estimator,

$$\boldsymbol{\sigma_y^2 = \left[\frac{median(|HH_1|)}{0.6745}\right]^2} \tag{4}$$

The variance of the degraded image can be estimated as:

$$\boldsymbol{\sigma_y^2 = \frac{1}{M}\sum_{m=1}^{M} A_m^2}\ , \tag{5}$$

where, A_m are the wavelet coefficients of wavelet on every scale; M is the total number of wavelet coefficient. Use of soft threshold which based on sub-band and level-dependent near-optimal threshold as equation condition for Bayes shrink thresholding:

$$T_{Bayes} = \begin{cases} \frac{\sigma_v^2}{\sigma_x} & if\ \sigma_v^2 < \sigma_y^2 \\ max(|A_m|) & otherwise \end{cases} \quad (6)$$

where

$$\sigma_x = \sqrt{\max(\sigma_y^2 - \sigma_v^2, 0)} \quad (7)$$

The basic framework of the wavelet transform based image de-noising is shown in Figure 4.

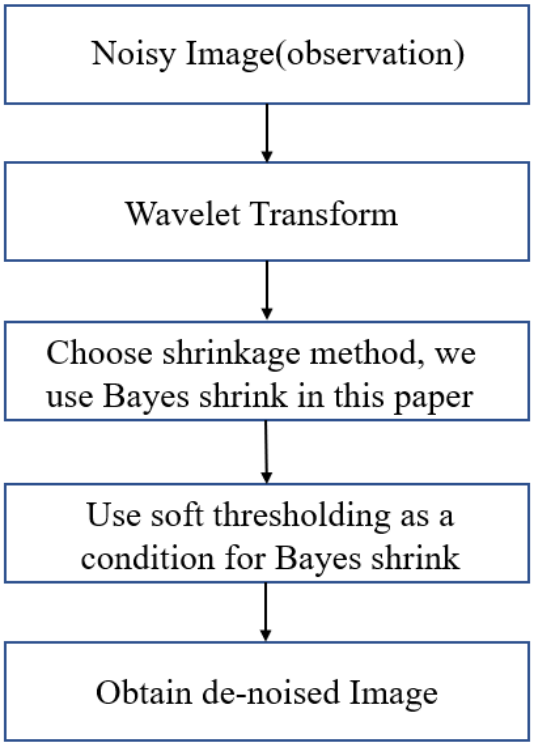

Figure 4. The basic framework of wavelet image de-noising. It shows the process of wavelet de-noising. There are three main steps. 1) Apply wavelet transform to image data and calculate the wavelet coefficients. 2) Find the optimum value for threshold and applying a soft threshold. 3) Calculate the de-noised signal and reconstruct the image.

3.2. Image segmentation:

The goal of this study is to identify the inundation or water area in CCTV images. To achieve this goal, the edge and contour of the object must be determined first using an image segmentation, which is an effective way to find the edge of the objects on the image. The classification of image segmentation is based on grayscale, color, texture, and shape to divide the image into several areas. The features that have been divided into the same area are similar, while there are significant differences between different areas. Moreover, this is the basis for image analysis and understanding of image feature extraction and object detection. There several image segmentation approaches are studied (e.g., region-based segmentation, clustering segmentation) *(31)* The region-

based segmentation divides the image into two regions of the target and the background by a single threshold. With different threshold calculation methods, the region-based segmentation presents different results. The clustering method is used to segment the image with the corresponding feature pixel points. The term “cluster” means that the area displays similar information based on surrounding pixels. For example, if a part of nearby pixels appear dark, the area called cluster will present dark information after image segmentation. According to their features in the cluster, the image is segmented into several different clusters in which each cluster has similar features. A global threshold can effectively segment different targets and backgrounds with different grayscales. However, when the grayscale difference of the image is not obvious, the local threshold or adaptive threshold method should be used. To be able to understand how the computer interprets images to detect an object's edge and find which image segmentation has the best performance to detect the water area, we use three different image-segmentation methods, which are k-means clustering segmentation, Otsu region-based segmentation, and Bayesian threshold segmentation.

3.2.1 k-means Segmentation:

Each pixel in a color image is a point in three-dimensional space; k-means segmentation uses pixels of the image as data points according to the specified number of clusters, replacing each pixel with its corresponding cluster center to reconstruct the image. k-means clustering minimizes the sum of the squared errors of the data in the cluster and the center of the cluster *(32)*. The purpose is to find a similar cluster in the data so that members in the same cluster have similar attributes. Assume there is a set of n-dimensional data:

$$x_i \in R^d, i = 1,2, \dots, n \; ; \; \{S_1, S_2, \dots, S_k\}, k \leq n \tag{8}$$

where x_i is set of i data points as the data to be clustered and d is a number of dimension of data points i; S_k is the number of clusters from data points x_i. By using the formula of Euclidean distance to calculate the sum of least squares between clusters center and pixel points x_i is the minimum value to define the number of clusters

$$\boldsymbol{arg_{\mu} min} \sum_{\boldsymbol{c=1}}^{\boldsymbol{k}} \sum_{\boldsymbol{i \in S_k}} ||\boldsymbol{x_i} - \boldsymbol{\mu_c}||^{\boldsymbol{2}} \, , \tag{9}$$

where μ_c is the center of k clusters and $arg_{\mu} min$ is the value of the variable μ_c reaches the minimum value in the following formula.

The image segmentation based on k-means uses the pixels as data points, using Equation (9) to calculate the number of clusters then replace each pixel with its corresponding cluster center to reconstruct the image. The different clusters present different colors and other characteristics, while the pixel points in the same cluster have similar characteristics.

3.2.2 Otsu Segmentation:

The most commonly used threshold segmentation algorithm is the most substantial interclass variance method (Otsu), which selects threshold by maximizing the variance between clusters. According to the grayscale characteristics of the image, Otsu assumes that the image is composed of two parts, the foreground and background. By calculating the variance of the foreground and background of the segmentation result under different thresholds, the threshold with the largest variance is the Otsu threshold *(33)*. The larger the between-class variance between the background and foreground, the better the effect to distinguish these two parts. The main calculated between-class variance equation is

$$g = \omega_1 * \omega_2 * (\mu_1 - \mu_2)^2 \tag{10}$$

where ω_1 and ω_2 are the ratio of background pixels and foreground pixels in the image, respectively; μ_1 and μ_2 are the average grayscale value of background and foreground.

3.2.3 Bayesian Segmentation:

Similar to Otsu segmentation, the image is divided into the foreground and background by Bayesian segmentation. The Bayesian theorem calculates the posterior probability with the smallest Bayesian risk as Bayesian shrink, which is defined as the probability distribution of expected values. Image segmentation is conditional assumption questions in which the decisions are usually based on probability to select value *(31, 34)*. If $P\left(\frac{H_0}{z}\right) > P\left(\frac{H_1}{z}\right)$, H_0 is selected; if $P\left(\frac{H_0}{z}\right) < P\left(\frac{H_1}{z}\right)$, then H_1 be chosen where P is a probability, H_0 and H_1 are decisions, and z is independently distributed Gaussian variables. For an image $I(m,n)$, the segmentation by using Bayesian theorem can be presented:

$$\boldsymbol{I(m,n) < \lambda : I(m,n) \in H_0} \tag{11}$$

$$\boldsymbol{I(m,n) \geq \lambda : I(m,n) \in H_1} \tag{12}$$

where λ is the Bayesian threshold of image and satisfies the following formula:

$$\frac{P\left(\frac{\lambda}{H_0}\right)}{P(H_0)} = \frac{P\left(\frac{\lambda}{H_1}\right)}{P(H_1)} \tag{13}$$

Assume that P(z) is the probability density function with the expected Bayesian threshold values of an image I(m, n), which is defined as the probability distribution based on Equations (11) to (13):

$$P(z) = P\left(\frac{z}{H_0}\right)P(H_0) + P\left(\frac{z}{H_1}\right)P(H_1) \quad (14)$$

For the image is divided into a background part ω_1 and target part ω_2 by a threshold, which their probability is $P(\omega_1)$ and $P(\omega_2)$, separately. The posterior probability can be present by Bayesian theorem:

$$\boldsymbol{P(\omega_i|x) = \frac{P(x|w_i)P(w_i)}{\sum_{j=1}^{2} P(x|w_j)P(w_j)}} \quad (15)$$

The threshold with minimum Bayesian risk has the maximum expectation of posterior probability represented by Equation (15), and can be written as:

$$\boldsymbol{T = \{x|\ P(w_1|x_0) = P(w_2|x_0)\}} \quad (16)$$

Based on threshold T presented on Equation (16), which has the maximum expectation of threshold based on the Bayesian theorem, the image segmentation results can get the minimum error, which means the distortion of the image after segmentation is minor.

4. FINDINGS

4.1 Data collection and Assessment Approach

4.1.1 Data Collection

In this study, 14 CCTV images which are collected from state website such as TranSTAR or downloaded from public social media have been tested to determine which de-noising method is the best for CCTV images. Six of the CCTV images are shown in Figure 5.

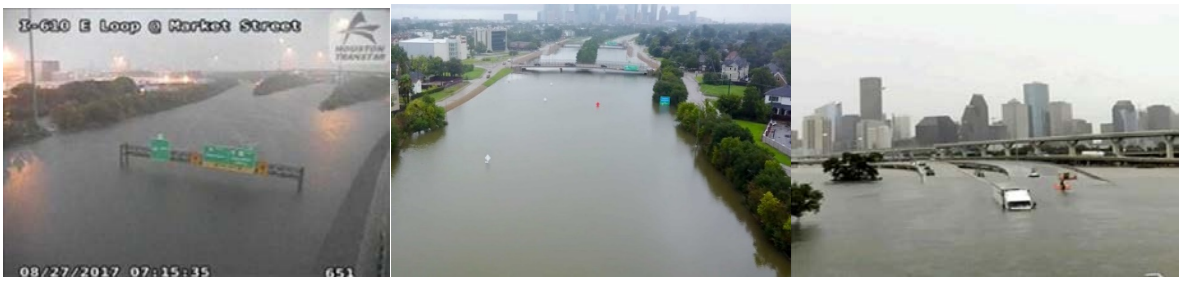

(a) Case No.1 (b) Case No.2 (c) Case No.3

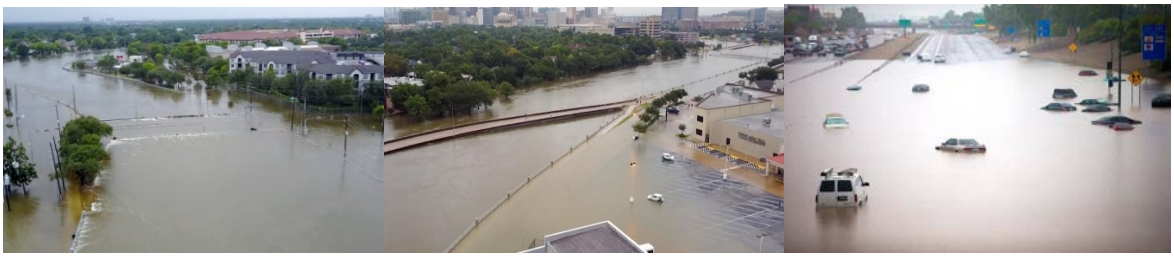

(d) Case No.4 (e) Case No.5 (f) Case No.6

Figure 5. Example images used for inundation detection experiments which are No. 1 to No. 6 in Table 1 collected from CCTV and social media used in this paper. (a) and (b) are flooded roads during Hurricane Harvey collected from CCTV; others are collected from social media.

4.1.2 Mean Squared Error (MSE) and Peak Signal-to-Noise Ratio (PSNR):

The quality and information of the image after compression or reconstruction are usually different from the original image. Image de-noising is also a process of compression and reconstruction, which can eliminate most image noise while maintaining image information. However, the differences are difficult to identify the performance of de-noising by the human eye. The criteria for the quality of de-noising filtering are determined by mean squared error (MSE) and peak signal-to-noise ratio (PSNR). MSE in mathematical statistics refers to the expected value of the squared difference between the estimated values and the true value, which can evaluate the degree of change of data. The smaller the value of MSE, the better the accuracy of the experimental data. PSNR is a measurement method to quantify the impact of image processing, which is commonly used for image compression and reconstruction after image de-noising. The higher the PSNR, the better the de-noising effect, and the more original image information is retained.

$$MSE = \frac{1}{mn}\sum_{i=0}^{m-1}\sum_{j=0}^{n-1}[I(i,j) - K(i,j)]^2 \quad (17)$$

$$PSNR = 10\log_{10}\frac{MAX_I^2}{MSE} = 20\log_{10}\frac{MAX_I}{MSE}, \quad (18)$$

where m, n is a resolution of image; $I(i,j)$ is an image after de-noise; $K(i,j)$ is a noisy image; MAX_I is the maximum of resolution (i.e., 8-bits image is 2^8 = 256 resolution). In theory, the de-noising method can only accurately remove image noise and retain the details of the image. The reconstructed image after de-noising must be consistent with the original image, except that it contains noise.

4.2 Results and Discussions

4.2.1 Efficiency of De-Noising Methods

The results of CCTV images via different de-noising methods are shown in Figure 6. According to this comparison Figure 6, the results demonstrate (b) the Bayes shrink is the best of these de-noising methods for CCTV images. It not only removes the noise but also retains important information, including brightness, color, and resolution of the original image. A reasonable explanation for the blurring of images after de-noising filtering like (c), (d) and (e) is the threshold applied in these methods is fixed, which means the threshold does not change with the important information of an image; therefore, the most important information is removed when the noise causes distortion of filtered images.

(a) Original CCTV image (Case No.1) (b) After Bayes shrink (Case No.1)

(c) After Arithmetic filtering(Case No.1) (d) After Median filtering (Case No.1)

(e) After Gaussian filtering (Case No.1)

Figure 6. The results of CCTV image (Case No.1 in Figure 6) via different de-noising methods: (a) Original CCTV image; (b) an image by using Bayes shrink; (c) an image by using Arithmetic filtering; (d) an image by using Median filtering and (e) an image by using Gaussian filtering. (b) Bayes shrink is the best of these de-noising method for CCTV images. It not only removes the noise but also retains important information, including brightness, color, and resolution of the original image.

In order to further verify the performance of de-noising methods, PSNR of each de-noising methods shown in Table1. The PSNR chart is shown in Figure 7, where the x-axis is the number of cases, and the y-axis is the percentage of PSNR. Based on the results, Bayes shrink has the best de-noising efficiency, which mostly PSNR is over 80db. In some cases, PSNR can reach over 85db. The results imply the similarity between the de-noised image and noisy image is 85%. Most image details can be preserved while the noise is accurately eliminated. For other filtering methods, which are median filtering, arithmetic filtering, and Gaussian filtering, their PSNR show around 20db to 30db, which means they have poor performance for de-noising. The results are so different between Bayes shrink and other methods because the threshold of the latter three methods are fixed instead of calculated by the image information such as Bayes shrink.

Table 1. The PSNR of each de-noising filtering

NO.	Bayes shrink wavelet coefficients (db)	Median filtering (db)	Arithmetic filtering (db)	Gaussian filtering (db)
1	83.60	36.05	22.64	23.13
2	80.94	32.87	20.83	20.70
3	83.36	34.70	21.58	20.98
4	79.99	31.74	21.15	20.30
5	79.92	32.39	22.22	20.87
6	79.03	32.06	20.68	19.16
7	87.15	39.31	26.68	27.34
8	81.07	32.80	23.93	24.38
9	80.25	28.73	21.36	20.92
10	81.30	29.47	21.04	20.99
11	86.71	33.92	20.65	21.88
12	85.59	33.45	20.28	20.42
13	89.15	34.25	22.54	22.76
14	89.68	33.52	20.92	19.69

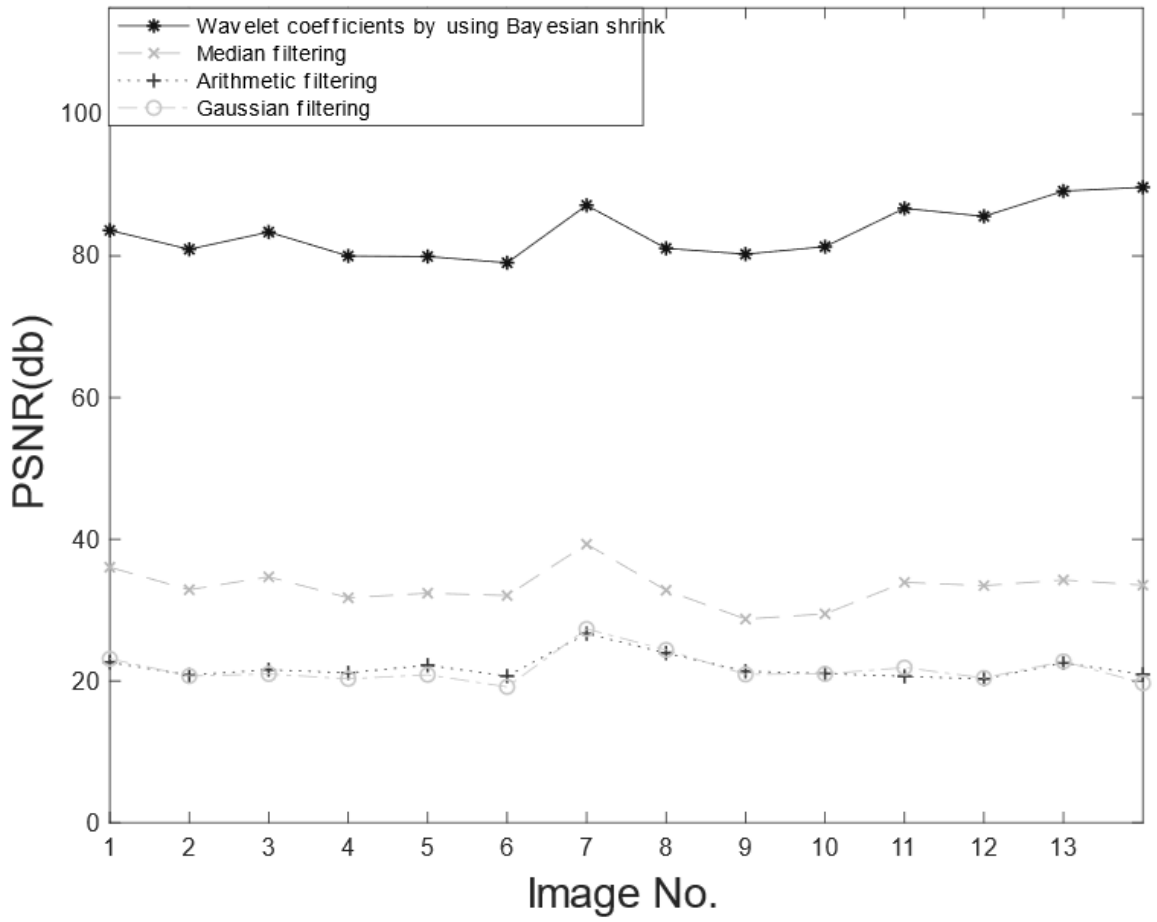

Figure 7. The chart of PSNR for each method with different 14 CCTV images. High PSNR indicates that the reconstructed image after de-noising retains the similar information of the original image, while most of the noise has been removed. Bayes shrink has the best de-noising performance since its PSNR average over 85db, which implies most image details can be preserved while the noise is accurately eliminated, as shown in Figure 6(b). On the other hand, the PSNR of other methods only around 20db to 40db, which means that most details of the original image have been deleted as noise. The de-noised image is distorted as shown in Figure 6 (c)(d)(e).

4.2.2 Detection of Inundation by Image Segmentation

Based on the results of de-noising shown in Table 1, the Bayes shrink has the best de-noising performance for CCTV image. The next step is to use image segmentation to determine whether these de-noised images are clear and can be used for computer analysis to detect object edge perfectly. This is one of the important keys to affect the subsequent image detection work and to identify the edge and contour of inundated water areas in the CCTV image. First, we use k-means segmentation, Otsu segmentation, and Bayesian segmentation methods to analyze images. An example from Figure 6; humans can easily identify the shape, brightness, and contrast of objects in the image. A computer recognizes pixel information and changes in pixels, which is very difficult unless computers can clearly distinguish areas with similar attributes before the

object detection procedure. Image segmentation helps us understand how computers parse images. The comparison of before and after image de-noising filtering is performed using three different image segmentation methods is shown in figure 8. More comparison of three different segmentation methods are presented in the appendix.

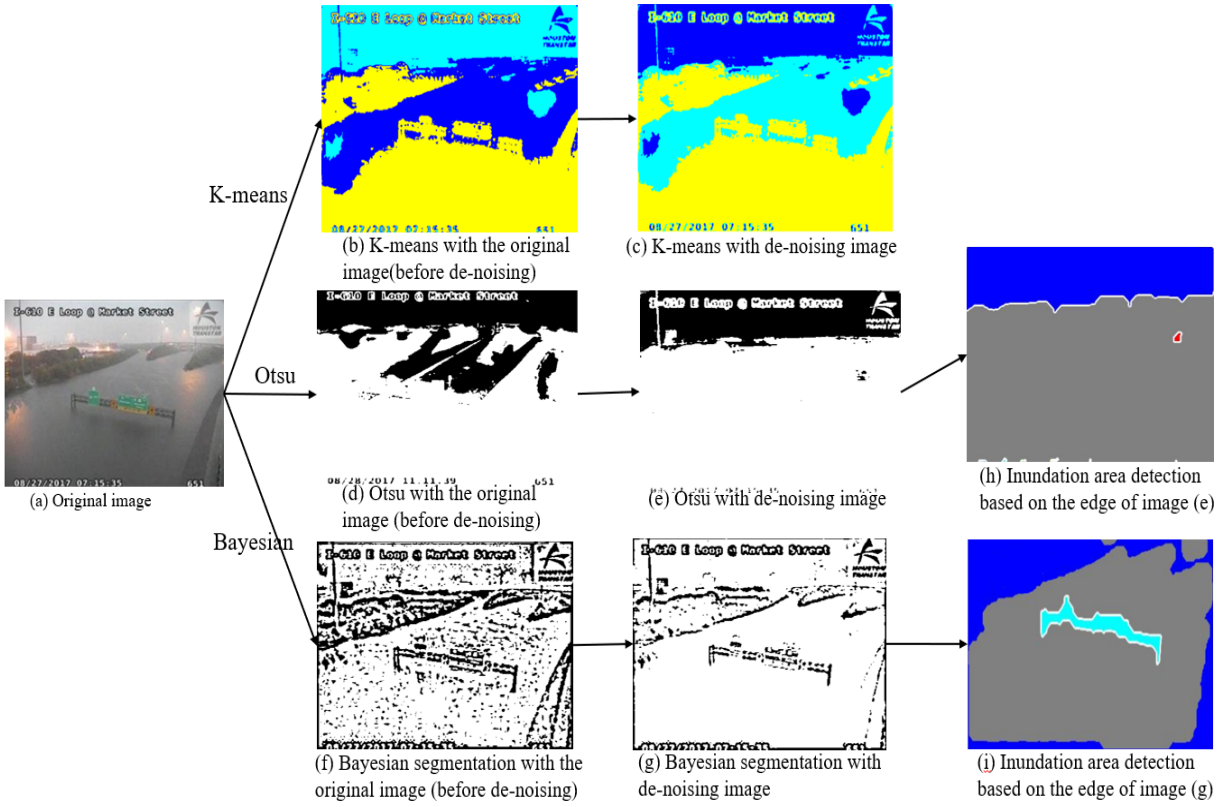

Figure 8. The comparison of before and after image de-noising filtering using different image segmentation methods. (b) and (c) are the results of using the k-means of the noisy image and the de-noised image; (d) and (e) are the results of using the Otsu of the noisy image and the de-noised image; and (f) and (g) are the results of using the Bayesian of the noisy image and the de-noised image, separately. (h) and (i) are water area surrounded by the edge of (e) and (g), separately.

Firstly, as shown in Figure 8, (b) and (c), the image using k-means segmentation is divided into different colors according to its attributes. It is clearly found that k-means cannot treat the water area as the same object with or without de-noising filtering. Thus, it indicates one part of water belongs to yellow, and the other part belongs to blue. The result of the Otsu image segmentation is shown in (d) and (e). Although it can detect mostly the water area, Otsu treats road parts as same as the water area so that all the images mostly in the same color, which is white. The results of Bayesian segmentation are shown in (f) and (g). There are many black spots in the image segmentation before de-noising filtering shown in (f) because those are noise. The result for Bayesian segmentation with the de-noised image shown in (g) shows that the computer can segment important information in the image (i.e., water and roads), which has the best performance among the three methods.

Secondly, based on the comparison results of (f) and (g), the importance of de-noising for image recognition can be determined. The Bayesian segmentation result with no de-noising image shown in (f), which has a lot of black dots, means there are pepper noise and (g) shows the Bayesian segmentation result with de-noised image, which shows perfect contour and edge of water area. By comparing two cases shown in (f) and (g), it is determined if the noise cannot be accurately removed, even accurate methods such as the Bayesian method that show poor image results.

In addition, to further compare the performance of each segmentation method, the inundation area detection is performed based on the Otsu segmentation (e) and Bayesian segmentation (g) shown in (h) and (i) which gray indicates water area and blue indicates other parts out of the area, while k-means already segment image (c) into colors—comparing the inundation area detection results with different segmentation methods, which are k-means, Otsu, and Bayesian segmentation shown in (c), (h), and (i), respectively. The inundation area detection based on Bayesian segmentation is the closest to the original image (a), which shows the perfect edge of the water area, while the other two results (c), (h) cannot display the correct inundation area corresponding to the original image (a). Summarizing the results shown in Figure 8, de-noising is important for image processing, which may affect the following processing results. Bayesian segmentation has the best performance to find inundation edges and using these edges to find the inundation area corresponding CCTV image. Consequently, there are two other images that use the edge based on Bayesian segmentation results to calculate inundation to achieve object detection.

The region of interest (ROI) for this study is the water area. The inundation detection results are shown in Figure 9, which presents the water area only. For Case No.2, which is shown in (a) and (b), the gray area indicates inundation while blue implies background outside the inundation area. For Case No.3, which is shown in (c) and (d), there are two different but similar colors at the top and bottom of (d). The gray at the top represents the sky, while the blue represents the background of the building, and the gray at the bottom represents the inundation. Compared with Case No. 2, there is a sky part in Case No. 3, which could affect object detection results for following work like use of a neural network to automatically identify whether there is inundation or not in the image. In this case, choosing the appropriate region of interest (ROI) is important, which controls the location of CCTV images to avoid sky part in the image to make inundation detection more accurately as shown as (e) and (f). The matching image of edge detection based on Bayesian segmentation result and original CCTV image shown in Figure 10. The result demonstrates high precision performance of Bayesian segmentation detection for inundation area.

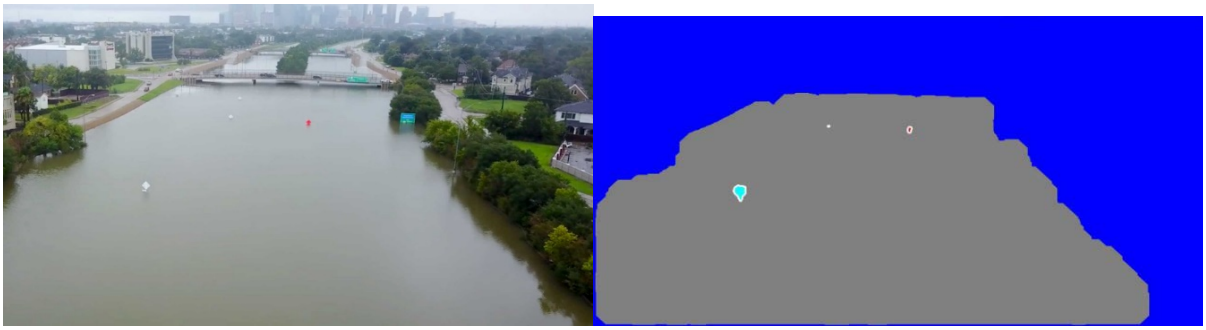

(a) CCTV image (Case No.2) (b) Inundation detection (Case No.2)

(c) CCTV image (Case No.3) (d) Inundation detection (Case No.3)

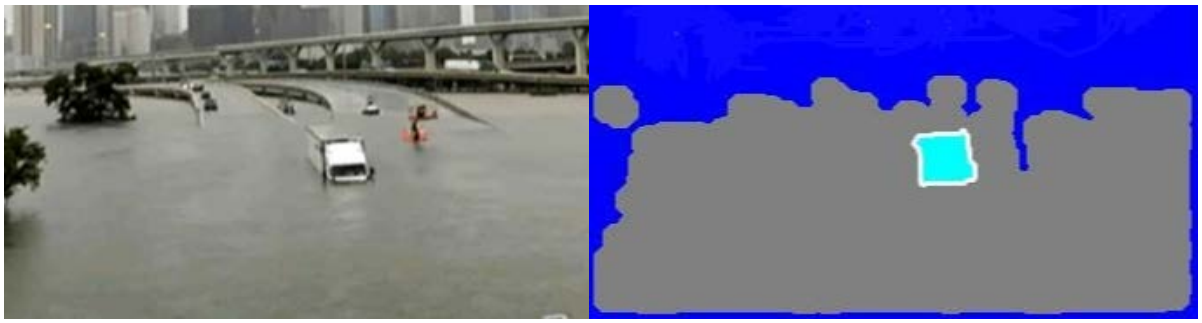

(e) ROI of Case No.3 by cutting the sky part (f) Inundation detection of (e)

Figure 9. Inundation detection is based on the results of Bayesian segmentation. To avoid detection errors, ROI should be chosen carefully. (e) is the image of cutting off the sky part of (c) which would be an error for inundation detection since in (d) the sky part and water part has the similar gray with means they have similar features for computer. After cutting the sky part, (f) shows only one gray for the water area; thus the accuracy of inundation detection could be increased.

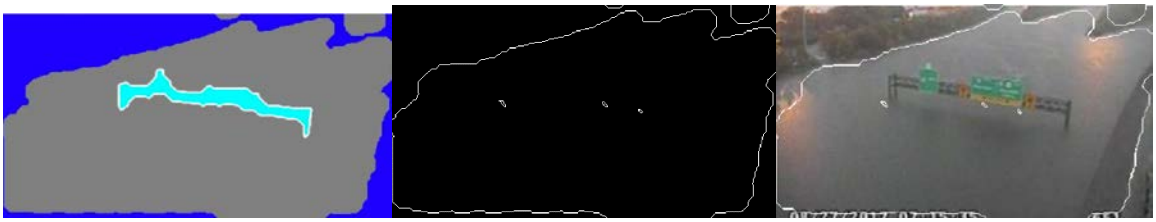

(a) Inundation detection (Case No.1)

(b) Edge detection based on Bayesian segmentation result (Case No.1)

(c) Matching image of edge detection and the original image (Case No.1)

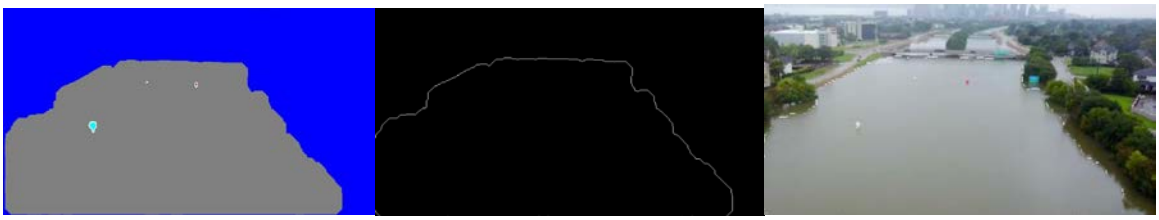

(d) Inundation detection (Case No.2)

(e) Edge detection based on Bayesian segmentation result (Case No.2)

(f) Matching image of edge detection and the original image (Case No.2)

(g) Inundation detection (Case No.3)

(h) Edge detection based on Bayesian segmentation result (Case No.3)

(i) Matching image of edge detection and the original image (Case No.3)

(j) Inundation detection (Case No.4)

(k) Edge detection based on Bayesian segmentation result (Case No.4)

(l) Matching image of edge detection and the original image (Case No.4)

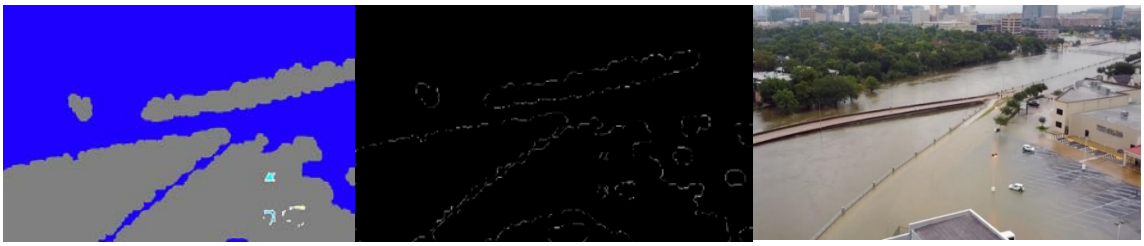

(m) Inundation detection (Case No.5)

(n) Edge detection based on Bayesian segmentation result (Case No.5)

(o) Matching image of edge detection and the original image (Case No.5)

(p) Inundation detection (Case No.6)

(q) Edge detection based on Bayesian segmentation result (Case No.6)

(r) Matching image of edge detection and the original image (Case No.6)

Figure 10. The matching image with edge detection based on Bayesian segmentation result and original CCTV image. (a)(d)(g)(j)(m)(p) are inundation detection by using Bayesian segmentation. (b)(e)(h)(k)(n)(q) are edge detection based on inundation detection (a)(d)(g)(j)(m)(p), respectively. (c)(f)(i)(l)(o)(r) are the matching image of edge detection and original CCTV image. The results show that the developed Bayesian segmentation has good ability to detect inundation area correctly.

4.3 Conclusions

In this study, we comparatively studied image-processing methods, such as de-noising methods and image segmentation, to automatically detect the flooded areas from the low-resolution images. The inundation detection results indicate that a series of methods are important and necessary to achieve detection. According to this research, the most effective de-noising method for a CCTV image is the Bayes shrink adaptive wavelet threshold. By using Bayes shrink and segmentation as a pre-processing procedure, future classification and object detection in CCTV images are expected to be more successful. The key findings are summarized below.

- First, by comparing the most recently used de-noising methods, Bayes shrink with adaptive wavelet coefficients shows the best de-noising performance of all indicating this by the minimum MSE and maximum PSNR for CCTV images. The PSNR of CCTV images, by using the Bayes shrink approach, mostly exceeds 85 dB, which means that at least 85 % of the image details are retained after de-noising.

- Second, for image-segmentation techniques, Bayesian segmentation has the best performance to find the inundation edge. The results present the most important part of following object detection. Bayesian segmentation allows identifying the inundation edges correctly in a grayscale image.

- Last, use of the edge based on Bayesian segmentation enabled us to calculate inundation to achieve object detection. We notice the importance of the ROI, which controls the location of CCTV images to avoid the sky part, which has similar features to the inundation part. In this study, the inundation in CCTV can be identified accurately, which is important for following work like water-level detection by using the coordinate of the image.

The image processing presented in this report is to estimate the inundation from images to assess flooding risks in the vicinity of the local flooding locations. Such information will help traffic engineers to take preventive or proactive actions to improve the safety of the drivers and to protect and preserve the transportation infrastructure.

For further research by using the concept of image processing presented in the research, which defines the edge of the inundation area, the depth of water can be calculated by the coordinate relationship between image and the real world. It is possible to monitor the inundation status and calculate the water level in real-time by using a traffic-monitoring camera in the future. This research demonstrates the other economical option for people to detect flooding conditions such as the location and water level of the inundation area to provide people with more and faster information. Moreover, the inundation depth result based on Bayesian segmentation filtering can be combined with existing flooding map to identify whether the real-time flood is too deep to maintain transportation and personnel safety.

REFERENCES

[1] R. Blessing, A. Sebastian, S. M. Asce, and S. D. Brody, "Flood Risk Delineation in the United States : How Much Loss Are We Capturing ?," vol. 18, no. 3, pp. 1–10, 2017.

[2] M. Mousa, X. Zhang, and C. Claudel, "Flash Flood Detection in Urban Cities Using Ultrasonic and Infrared Sensors," *IEEE Sens. J.*, vol. 16, no. 19, pp. 7204–7216, 2016.

[3] L. Alfieri, D. Velasco, and J. Thielen, "Flash flood detection through a multi-stage probabilistic warning system for heavy precipitation events," *Adv. Geosci.*, vol. 29, no. 1, pp. 69–75, 2011.

[4] S. J. Noh, J. H. Lee, S. Lee, and D. J. Seo, "Retrospective dynamic inundation mapping of hurricane harvey flooding in the Houston metropolitan area using high-resolution modeling and high-performance computing," *Water (Switzerland)*, vol. 11, no. 3, 2019.

[5] S. W. Lo, J. H. Wu, F. P. Lin, and C. H. Hsu, "Visual Sensing for Urban Flood Monitoring," *Sensors (Switzerland)*, vol. 15, no. 8, pp. 20006–20029, 2015.

[6] S. Van Ackere, J. Verbeurgt, L. De Sloover, S. Gautama, A. De Wulf, and P. De Maeyer, "A Review of the Internet of Floods: Near Real-Time Detection of a Flood Event and Its Impact," *Water (Switzerland)*, vol. 11, no. 11, pp. 1–26, 2019.

[7] J. Xie, L. Xu, and E. Chen, "Image Denoising and Inpainting with Deep Neural Networks," *Adv. Neural Inf. Process. Syst. 25 (NIPS 2012)*, pp. 1–9, 2012.

[8] A. Buades, B. Coll, and J. M. Morel, "A review of image denoising algorithms, with a new one," *Multiscale Model. Simul.*, vol. 4, no. 2, pp. 490–530, 2005.

[9] Y. Zhu and C. Huang, "An Improved Median Filtering Algorithm for Image Noise," *Phys. Procedia*, vol. 25, pp. 609–616, 2012.

[10] M. Kazubek, "Wavelet domain image denoising by thresholding and Wiener filtering," *IEEE Signal Process. Lett.*, vol. 10, no. 11, pp. 324–326, 2003.

[11] D. L. Donoho, I. M. Johnstone, G. Kerkyacharian, and D. Picard, "Wavelet Shrinkage : Asymptopia," *J. R. Stat. Soc.*, pp. 1–45, 1995.

[12] D. L. Donoho and L. M. Johnstone, "Adapting to Unknown Smoothness via Wavelet Shrinkage," *Fundam. Pap. Wavelet Theory*, pp. 856–833, 1994.

[13] D. L. Donoho, "De-Noising by Soft-Thresholding," *IEEE Trans. Inf. Theory*, vol. 41, no. 3, pp. 631–637, 1995.

[14] J. Portilla, V. Strela, M. J. Wainwright, and E. P. Simoncelli, "Adaptive Wiener denoising using a Gaussian scale mixture model in the wavelet domain," *IEEE Int. Conf. Image Process.*, vol. 2, no. May 2014, pp. 37–40, 2001.

[15] S. G. Chang, B. Yu, and M. Vetterli, "Adaptive Wavelet Thresholding for Image Denoising and Compression," *IEEE Transactions on Image Processing*, 2000. .

[16] R. D. Nowak, "Wavelet-based Rician noise removal for magnetic resonance imaging," *IEEE Trans. Image Process.*, vol. 8, no. 10, pp. 1408–1419, 1999.

[17] S. G. Mallat, "A Theory for Multiresolution Signal Decomposition: The Wavelet Representation," *IEEE Trans. Pattern Anal. Mach. Intell.*, vol. 11, no. 7, pp. 674–693, 1989.

[18] S. Mallat and W. L. Hwang, “Singularity Detection and Processing with Wavelets,” *IEEE Transactions on Information Theory*, vol. 38, no. 2. pp. 617–643, 1992.

[19] K. Tharani, C. Mani, and I. Arora, “A Comparative Study of Image Denoising Methods Using Wavelet Thresholding Techniques,” *Int. J. Eng. Res. Appl.*, vol. 6, no. 12, pp. 73–77, 2016.

[20] J. Dijk and R. J. M. den Hollander, “Image enhancement for noisy color imagery,” in *Electro-Optical and Infrared Systems: Technology and Applications V*, 2008, vol. 7113, no. October 2015, p. 71131A.

[21] P. F. Felzenszwalb and D. P. Huttenlocher, “Efficient graph-based image segmentation,” *Int. J. Comput. Vis.*, vol. 59, no. 2, pp. 167–181, 2004.

[22] J. Y. Kim, L. S. Kim, and S. H. Hwang, “An advanced contrast enhancement using partially overlapped sub-block histogram equalization,” *IEEE Trans. Circuits Syst. Video Technol.*, vol. 11, no. 4, pp. 475–484, 2001.

[23] M. Abdullah-Al-Wadud, M. H. Kabir, M. A. A. Dewan, and O. Chae, “A dynamic histogram equalization for image contrast enhancement,” *IEEE Trans. Consum. Electron.*, vol. 53, no. 2, pp. 593–600, 2007.

[24] T. s. Huang;, G. J. Yang;, and Gregory Y. Tang, “A Fast Two-Dimensional Median Filtering Algorithm,” *IEEE Trans. Image Process.*, vol. 27, no. 1, 1979.

[25] H. Hwang and R. A. Haddad, “Adaptive Median Filters,” *IEEE Trans. Image Process.*, vol. 4, no. 4, pp. 7–10, 1995.

[26] G. Deng and L. W. Cahill, “An Adaptive Gaussian Filter For Noise Reduction and Edge Detection,” in *Nuclear Science Symposium and Medical Imaging Conference, 1993., 1993 IEEE Conference Record.*, 1993, no. January 1993.

[27] S. Sardy, P. Tseng, and A. Bruce, “Robust Wavelet Denoising,” *IEEE Trans. Image Process.*, vol. 49, no. 6, pp. 1146–1152, 2001.

[28] J. M. Shapiro, “Embedded image coding using zerotrees of wavelet coefficients,” in *Fundamental Papers in Wavelet Theory*, vol. 41, no. 92, 2009, pp. 861–878.

[29] S. Mallat, *A Wavelet Tour of Signal Processing*. 1999.

[30] S. G. Chang, B. Yu, and M. Vetterli, “Spatially Adaptive Wavelet Thresholding with Context Modeling for Image Denoising,” *IEEE Trans. Image Process.*, vol. 9, no. 9, pp. 1522–1531, 2000.

[31] M. Pereyra and S. McLaughlin, “Fast Unsupervised Bayesian Image Segmentation with Adaptive Spatial Regularisation,” *IEEE Trans. Image Process.*, vol. 26, no. 6, pp. 2577–2587, 2017.

[32] H. P. Ng, S. H. Ong, K. W. C. Foong, P. S. Goh, and W. L. Nowinski, “Medical Image Segmentation Using K-Means Clustering and Improved Watershed Algorithm View project Neuro vasculature modeling View project MEDICAL IMAGE SEGMENTATION USING K-MEANS CLUSTERING AND IMPROVED WATERSHED ALGORITHM,” *2006 IEEE Southwest Symp. Image Anal. Interpret.*, no. February 2001, pp. 61–65, 2001.

[33] T. Kurita, N. Otsu, and N. Abdelmalek, “Maximum Likelihood Thresholding Based on

Population Mixture Models," *Pattern Recognit.*, vol. 25, no. 10, pp. 1231–1240, 1992.

[34] C. A. Bouman and M. Shapiro, "A Multiscale Random Field Model for Bayesian Image Segmentation," *IEEE Trans. Image Process.*, vol. 3, no. 2, pp. 162–177, 1996.

APPENDIX: Analysis data and filtered data

(a) Original CCTV image (b) OTSU segmentation result

(c) K-means segmentation result (d) Developed Bayesian segmentation result

Figure A1. Analysis data(original CCTV image) and filtered data

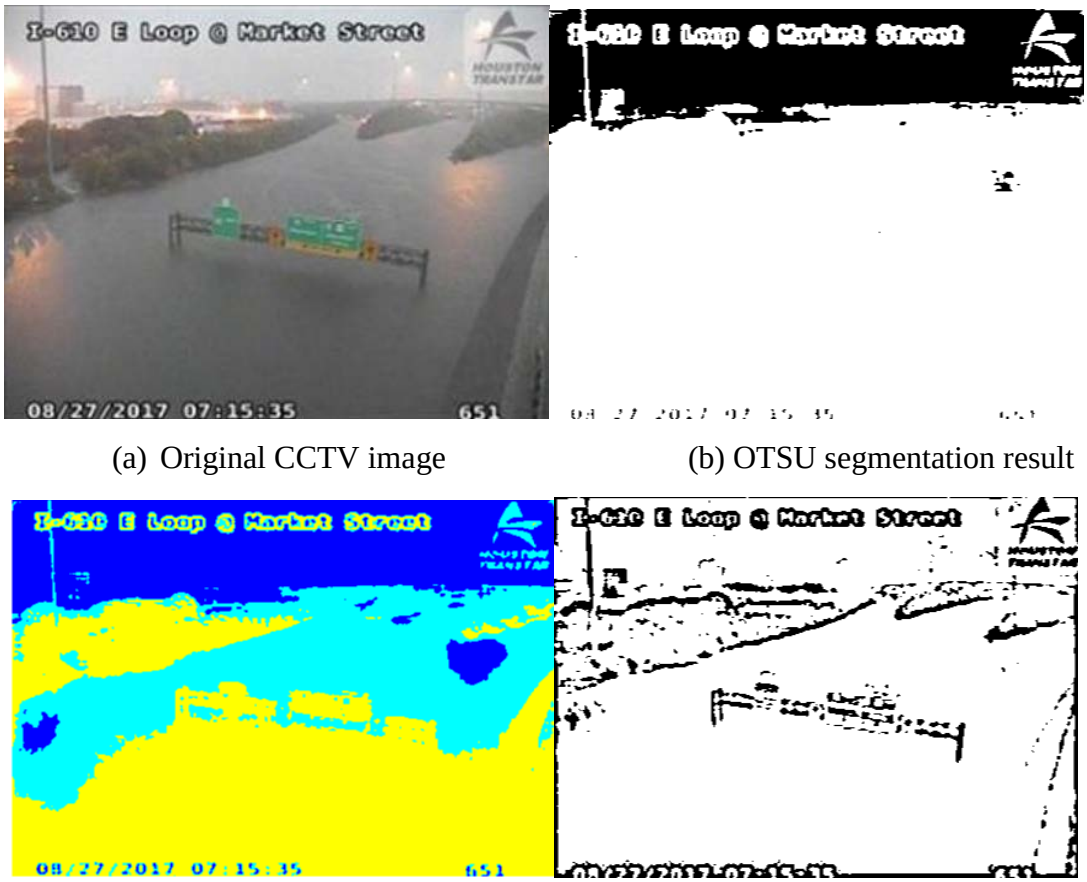

(a) Original CCTV image (b) OTSU segmentation result

(c) K-means segmentation result (d) Developed Bayesian segmentation result

Figure A2. Analysis data(original CCTV image) and filtered data

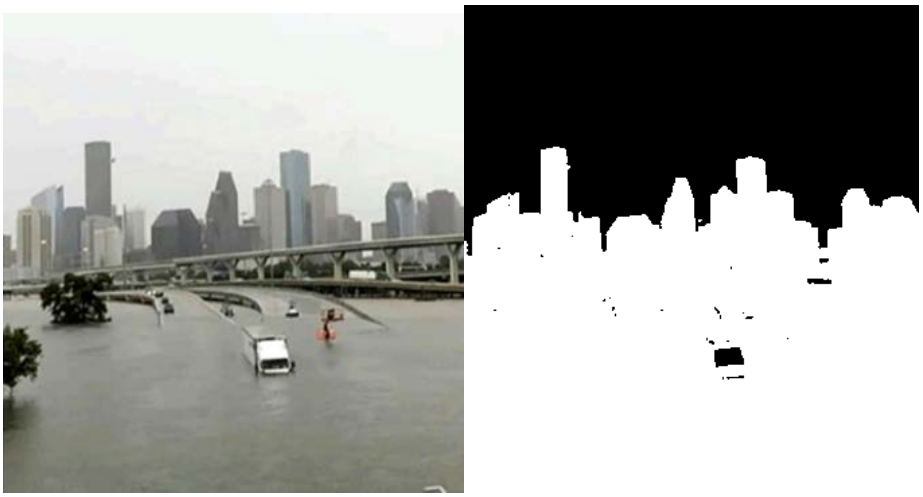

(a) Original CCTV image (b) OTSU segmentation result

(c) K-means segmentation result (d) Developed Bayesian segmentation result

Figure A3. Analysis data(original CCTV image) and filtered data

(a) Original CCTV image

(b) OTSU segmentation result

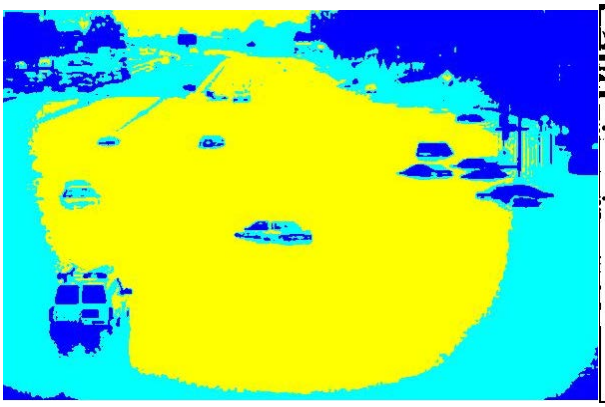

(c) K-means segmentation result

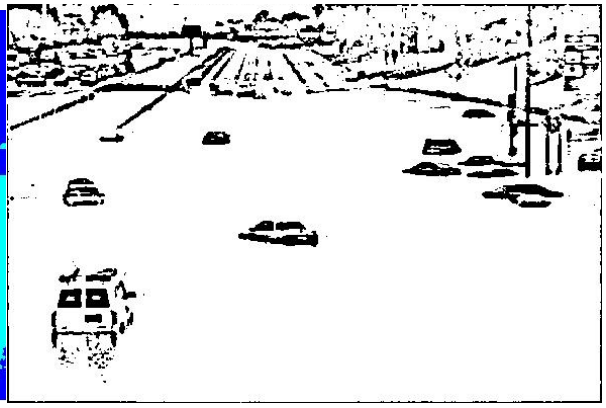

(d) Developed Bayesian segmentation result

Figure A4. Analysis data(original CCTV image) and filtered data

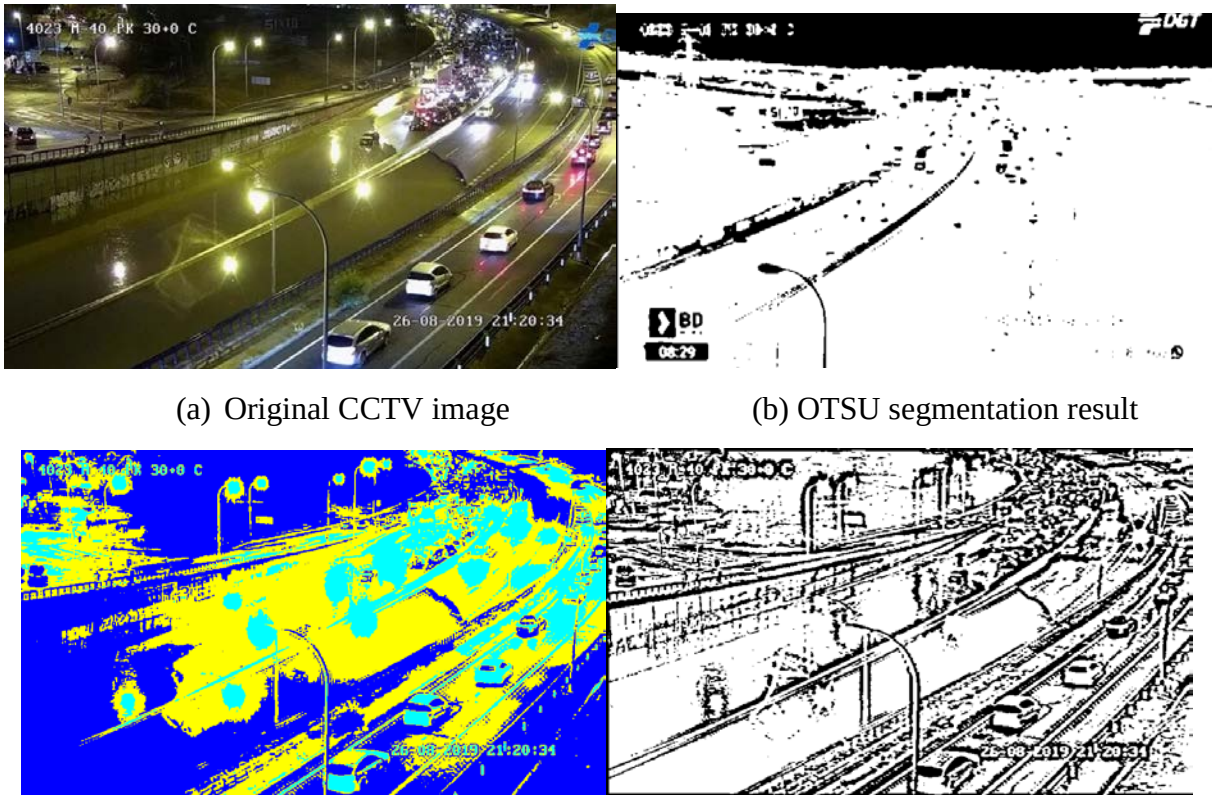

(a) Original CCTV image (b) OTSU segmentation result

(c) K-means segmentation result (d) Developed Bayesian segmentation result

Figure A5. Analysis data(original CCTV image) and filtered data

(a) Original CCTV image (b) OTSU segmentation result

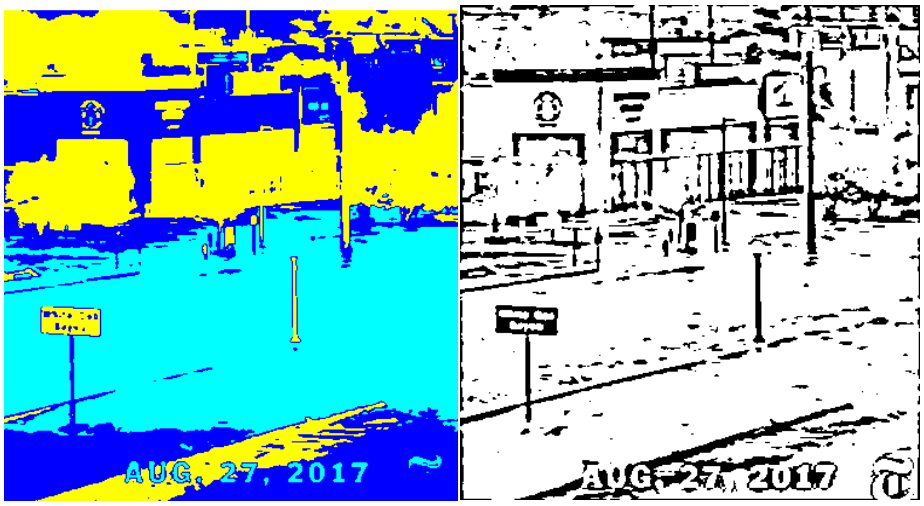

(c) K-means segmentation result (d) Developed Bayesian segmentation result

Figure A6. Analysis data(original CCTV image) and filtered data

(a) Original CCTV image (b) OTSU segmentation result

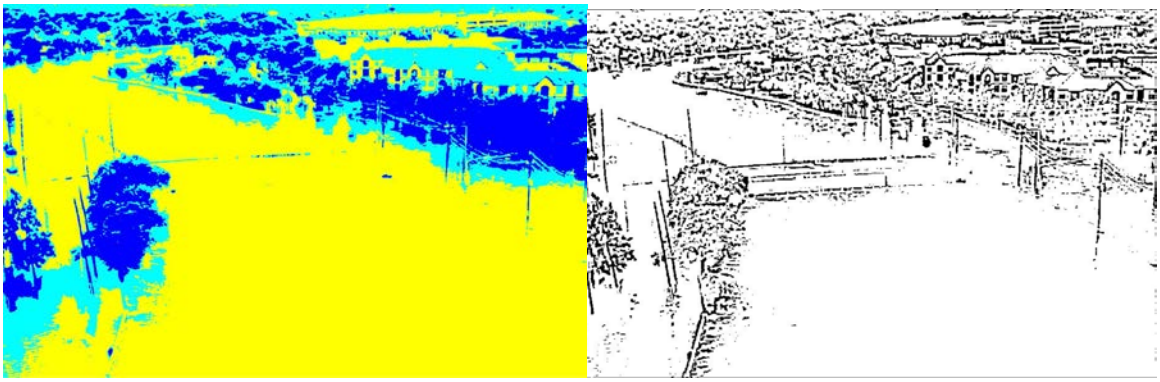

(c) K-means segmentation result (d) Developed Bayesian segmentation result

Figure A7. Analysis data(original CCTV image) and filtered data